J. Synchrotron Rad. (1998). **5**, 521–523

Commissioning and first results of the LNLS XAFS beamline

H. Tolentino,* J. C. Cezar, D. Z. Cruz, V. Compagnon-Cailhol, E. Tamura and M. C. Martins Alves

Laboratorio Nacional de Luz Sincrotron LNLS/CNPq, Caixa Postal 6192, 13083-970 Campinas (SP), Brazil. E-mail: helio@lnls.br

(*Received 4 August 1997; accepted 3 November 1997*)

An X-ray absorption fine-structure spectroscopy beamline has been installed and commissioned at a bending-magnet source at LNLS. Three monochromators are available: a channel-cut, a double-crystal and a four-crystal set-up. They have been operated from 2500 up to 15 000 eV, with a resolving power better than 5500 in the full range. Photon flux of the order of 10^8 photons s^{-1} up to 10^{10} photons s^{-1} has been attained. The experimental station is equipped with a table that can withstand a weight of 300 kg and track the vertical position of the beam with a 2.5 μm accuracy over a 120 mm stroke. The beamline has been fully characterized and the first results are presented.

Keywords: XAFS; beamline optics; instrumentation.

1. Introduction

We present the commissioning and very first results of the XAFS beamline installed at LNLS in Campinas, Brazil. The LNLS synchrotron radiation source is composed of a 1.37 GeV storage ring and a 120 MeV linac. The storage ring is a third-generation light source with a critical energy of 2.08 keV. The natural emittance is 100 nm rad and the revolution frequency is 3.2 MHz for this 93.2 m-long machine (Rodrigues *et al.*, 1997). The storage ring has been commissioned and reached the target parameters of 100 mA at 1.37 GeV. Up to now, the average lifetime is about 5 h and a lifetime of 10 h is expected to be reached within this year.

2. Beamline description

The design and performance testing of most elements of the XAFS beamline have been performed entirely at LNLS. The main components of the beamline are (Fig. 1): (i) bending-magnet source, (ii) front end, (iii) mirror chamber, (iv) the monochromator, and (v) experimental station. In addition, there are three sets of slits, two 125 μm-thick Be windows and one 50 μm-thick Kapton window at the end of the line. The first Be window isolates the UHV vacuum of the storage ring and front end from the vacuum of the mirror chamber, maintained at a pressure below 10^{-7} torr. The second Be window isolates the mirror chamber from the monochromator, maintained at a pressure of 10^{-3} torr by a mechanical pump. It is planned for the near future to eliminate one Be window and to operate the monochromator at a base pressure below 10^{-7} torr. For the first year of operation we have decided to operate the beamline without a mirror. The horizontal and vertical dimensions (FWHM) of the source are 695 and 165 μm, respectively. The vertical divergence is 370 μrad at the critical energy, limited by $1/\gamma$. The maximum horizontal acceptance, defined by the mask in the front end, is 8 mrad.

The monochromator chamber and goniometer can accept three different mountings: a channel-cut crystal, a double-crystal and a high-resolution four-crystal monochromator. The rotation of the goniometer is achieved by a single high-precision translation stage connected to a drum by a thin steel wire. The translation stage with 0.5 μm $step^{-1}$ along with a drum of 200 mm diameter produces an angular resolution of 5 μrad $step^{-1}$. The goniometer can cover a 90° range. The useful angular range, due to limitations on crystal dimensions, starts around 7° and goes up to 80°. Complete descriptions of the double-crystal and four-crystal monochromators are given in a previous paper (Tolentino *et al.*, 1995).

The monochromator has been used from 2500 eV up to 15 000 eV, with a photon intensity of the order of 10^8 photons s^{-1} up to 10^{10} photons s^{-1}. The measured photon intensity delivered by an Si(111) channel-cut crystal using a 100% efficiency photodiode placed just after the endstation Kapton window is reported in Fig. 2. Entrance monochromator slits were set to 0.5 and 1.5 mm for the vertical and horizontal directions, respectively. This gives 0.05 mrad vertical and 0.141 mrad horizontal acceptances. The reported photon intensity was measured for a ring current of 37 mA; it has been normalized to 100 mA, the nominal ring current. The decreasing intensity on the high-energy side is as expected for our low-energy machine. The low-energy

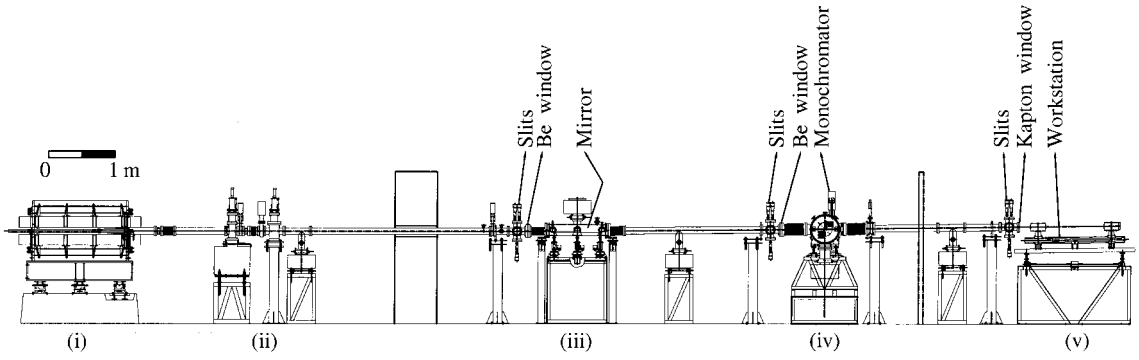

Figure 1
View of the XAFS beamline: (i) bending-magnet source, (ii) front end, (iii) mirror chamber, (iv) monochromator, and (v) workstation. There are three sets of slits, two 125 μm Be windows and one 50 μm Kapton window along the whole beamline.

side is limited by the windows. Below 3 keV, the harmonic contamination starts to become important, as can be observed by the unexpected increase in the photon intensity. In order to eradicate these contaminations we have to use either the double-crystal set-up or install the mirror. The useful range for the channel-cut crystal turns out to be 3000–15 000 eV.

The energy resolution can be derived from Bragg's law and is given by $\Delta E/E = \Delta\theta \cot\theta_B$, where $\Delta\theta$ is determined by the vertical angular spread of the incident beam and the intrinsic reflection width. To evaluate energy resolution we looked at a very sharp feature of the absorption spectrum of $KMnO_4$. This feature comes from the mixing of the 3*d* and 4*p* orbitals of the tetrahedral symmetry and represents the projection of the 3*d* quasi-localized states on the *p* bands (Mehadji *et al.*, 1990). The core-hole width of the Mn *K*-edge is about 1.1 eV and imposes a lower limit for any feature in its spectrum. The measured energy spread was 1.6 eV at 6550 eV (Fig. 3), so that we deduce an experimental resolution of 1.2 eV, *i.e.* $\Delta E/E = 1.8 \times 10^{-4}$, or a resolving power of 5500. This can be improved by going to higher-order reflections and/or to the four-crystal set-up, where the resolving power for the same Si(111) reflection is about 8000.

In the double-crystal monochromator, the fine adjustment of the parallelism between the crystals is performed by a solenoid and a small permanent magnet with an accuracy better than 0.1 arcsec. This has been used to measure rocking curves and to set the detuning to eradicate harmonic contamination. Not only the detuning, but the whole monochromator setting, bears on the stability of that mechanism. The short- and long-term stability have been measured at 8.7 keV using the Si(333) reflection. Aluminium foils were used to decrease the fundamental reflection Si(111). If we assign the small intensity decay (Fig. 4) to an angular variation, the short-term stability gives a figure of less than 0.1 arcsec variation within 15 min. If we take into account the beam decay, the figure is much better. The stability, reproducibility and accuracy of the energy calibration have been verified by scanning the same edge several times. For spectra taken one after the other, separated by less than 10 min, the accuracy is around 2 µrad, which gives a figure of 75 meV at the Cu *K*-edge. The long-term accuracy is worse than that, being as much as 10 µrad, and has been correlated to beam instabilities.

The experimental station is equipped with a table that can stand a maximum weight of 300 kg and track the vertical position of the beam with a 2.5 µm accuracy over a 120 mm stroke. Ion chambers, photodiodes, He-flow electron (Tourillon *et al.*, 1987) and fluorescence (Lytle *et al.*, 1984) detectors have been used in experiments. These detectors and an *XY* remote-controlled sample holder stand on a 1.60 m-long rail aligned to the beam direction. Cryostats (10–300 K and 80–700 K), magnetic fields (0.9 T), furnaces (up to 1500 K) and electrochemical cells will be available as sample environments.

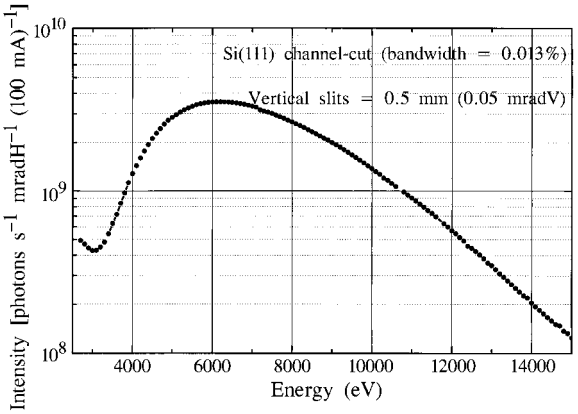

Figure 2
Measured photon intensity delivered by an Si(111) channel-cut crystal using a 100% efficiency photodiode.

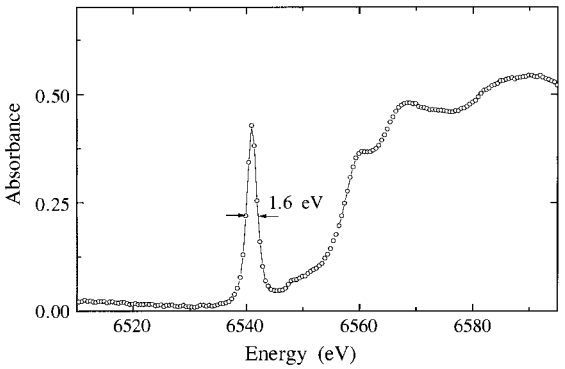

Figure 3
Mn *K*-edge of $KMnO_4$ using an Si(111) channel-cut monochromator. The sharp (1.6 eV) pre-edge feature allows an experimental energy resolution of 1.2 eV, or a resolving power ($E/\Delta E$) of 5500, to be estimated. LNLS: 1.37 GeV; 10.5 mA; 180 min. Accepted beam = 0.05 mrad (V) × 0.2 mrad (H).

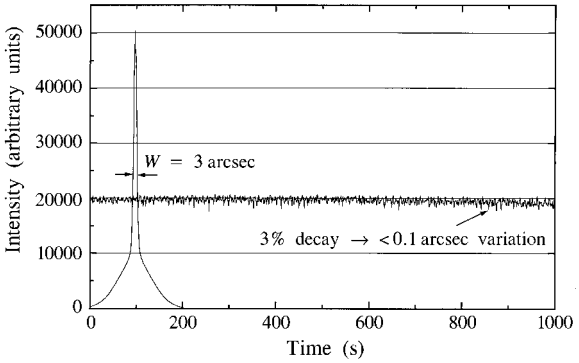

Figure 4
Short-term stability of the double-crystal monochromator measured at the steepest position of the Si(333) reflection for 8.7 keV photons. E = 1.37 GeV; I = 20 mA; τ = 180 min.

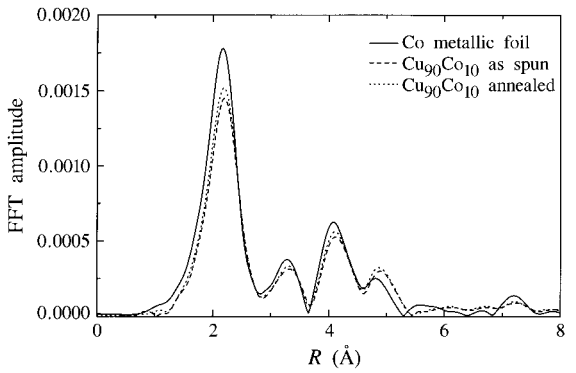

Figure 5
Fourier transforms of EXAFS signal at the Co *K*-edge of Co foil and of melt-spun $Co_{10}Cu_{90}$ alloys, for as-cast and annealed samples.

3. First results

Co nanoparticles embedded in a Cu matrix display large magnetoresistance, depending on the Co content and on the thermal treatment (Allia *et al.*, 1994). Melt-spun Co/Cu alloys, with different concentrations, were submitted to Joule thermal annealing, with a steady current, and studied by EXAFS. The edge features and extended oscillations of these cobalt nanoparticles are quite similar to those of Co metal, indicating that these Co/Cu alloys are forming well crystallized samples. The Fourier transforms (Fig. 5) are in agreement with this assumption. However, the Fourier transform amplitudes are smaller than in bulk Co, indicating a reduction in the coordination number. This question has to be investigated in more detail.

The XMCD signal is defined, for a given circularly polarized state, by the difference in absorption when the direction of the magnetization along the X-ray propagation is changed. The first test measurement on XMCD has been carried out on the L_3-edge of a $GdCo_3$ amorphous thin film, which saturates at about 0.5 T (Bonfim *et al.*, 1998). The film is slightly anisotropic with an easy axis of magnetization in the plane of the film. We have used an NdFeB permanent magnet to apply a 0.2 T field perpendicular to the film. The entrance vertical slits were set to accept 0.06 mrad at 0.22 mrad above the plane of the orbit. The expected circular polarization ratio is 30%. The horizontal slits were set to 0.5 mrad, giving a beam size at the sample of 0.9×8 mm. The XMCD signal appears from the difference in absorption by changing the direction of the magnetic field along the X-ray propagation. This has been obtained by simple 180° rotation of the sample holder. The normalized absorption and XMCD signal (Fig. 6) come from an average of four spectra for each orientation taken with the Si(111) channel-cut monochromator, with an energy step of 0.8 eV, 1 s point^{-1}. The LNLS storage ring was running at 1.37 GeV and 58 mA.

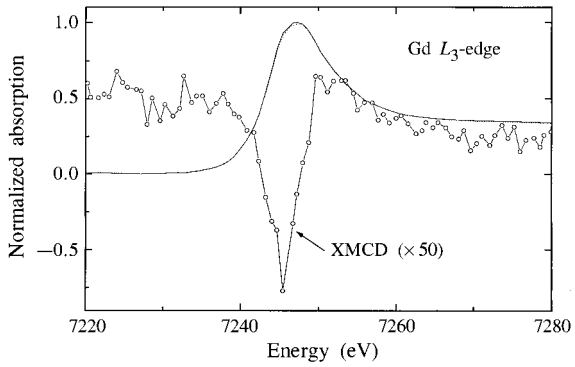

Figure 6
Normalized Gd L_3-edge absorption of $GdCo_3$ and XMCD signal.

References

Allia, P., Beatrice, C., Knobel, M., Tiberto, P. & Vinai, F. (1994). *J. Appl. Phys.* **76**, 6817–6819.

Bonfim, M., Mackay, K., Pizzini, S., San Miguel, A., Tolentino, H., Giles, C., Neisius, T., Hagelstein, M., Baudelet, F., Malgrange, C. & Fontaine, A. (1998). *J. Synchrotron Rad.* **5**, 750–752.

Lytle, F. W., Greegor, R. B., Sandstrom, D. R., Marques, E. C., Wong, J., Spiro, C. L., Huffman, G. P. & Huggins, F. E. (1984). *Nucl. Instrum. Methods*, A**226**, 542–548.

Mehadji, C., Nour, S., Chermette, H., Cartier, C., Menage, S. & Verdaguer, M. (1990). *Chem. Phys.* **148**, 95–102.

Rodrigues, A. R. D., Farias, R. H. A., Ferreira, M. J., Franco, G. S., Janhnel, L. C., Lin, L., Lira, A. C., Neuenschwander, R. T., Pardine, C., Rafael, F., Rosa, A., Scorzato, C., Gonçalves da Silva, C. E. T., Romeu da Silva, A., Tavares, P. F., Wisnivesky, D. & Craievich, A. (1997). *Particle Accelerator Conference*, Vancouver, Canada.

Tolentino, H., Durr, J., Mazzaro, I., Udron, D. & Cusatis, C. (1995). *Rev. Sci. Instrum.* **66**, 1806–1808.

Tourillon, G., Dartyge, E., Fontaine, A., Lemonnier, M. & Bartol, F. (1987). *Phys. Lett. A*, **121**, 251–257.